The Meteoritical Society

Meteoritics & Planetary Science 52, Nr 6, 1216–1232 (2017)
doi: 10.1111/maps.12845

Revising the shock classification of meteorites

Jörg FRITZ[1,*], Ansgar GRESHAKE[2], and Vera A. FERNANDES[2]

[1]Saalbau Weltraum Projekt, Liebigstrasse 6, 64646 Heppenheim, Germany
[2]Museum für Naturkunde Berlin, Invalidenstrasse 43, 10115 Berlin, Germany
[*]Corresponding author. E-mail: joerg.fritz@kino-heppenheim.de

(Received 16 March 2016; revision accepted 18 January 2017)

Abstract–The current shock classification scheme of meteorites assigns shock levels of S1 (unshocked) to S6 (very strongly shocked) using shock effects in rock-forming minerals such as olivine and plagioclase. The S6 stage (55–90 GPa; 850–1750 °C) relies solely on localized effects in or near melt zones, the recrystallization of olivine, or the presence of mafic high-pressure phases such as ringwoodite. However, high whole rock temperatures and the presence of high-pressure phases that are unstable at those temperatures and pressures of zero GPa (e.g., ringwoodite) are two criteria that exclude each other. Each type of high-pressure phase provides a minimum shock pressure during elevated pressure conditions to allow the formation of this phase, and a maximum temperature of the whole rock after decompression to allow the preservation of this phase. Rocks classified as S6 are characterized not by the presence but by the absence of those thermally unstable high-pressure phases. High-pressure phases in or attached to shock melt zones form mainly during shock pressure decline. This is because shocked rocks (<60 GPa) experience a shock wave with a broad isobaric pressure plateau only during low velocity (<4.5 km s^{-1}) impacts, which rarely occur on small planetary bodies; e.g., the Moon and asteroids. The mineralogy of shock melt zones provides information on the shape and temporal duration of the shock wave but no information on the general maximum shock pressure in the whole rock.

INTRODUCTION

Meteorites represent unique samples from different types of planetary bodies allowing the study of the formation and evolution of planetary bodies, the history of the solar system (McSween 1999; Wood 2005; Fritz et al. 2014) and, to some extent, the presolar stars, which produced the elements of which the solar system is made (Wasserburg et al. 2006; Ott [2007] and references therein). Meteorites from primitive and differentiated parent bodies are fragments derived by collisions. Most meteorites accessible for scientific analysis experienced hypervelocity collisions that drove shock waves through the rock (Stöffler et al. 1991; Rubin 2015).

A shock wave in a solid is a compressional wave with an amplitude that exceeds the elastic limit of the material in which it propagates (Doran and Linde 1966). The resulting shock-induced pressure and temperature increase produce characteristic modifications in the minerals constituting the rock. These effects are collectively called shock metamorphism. To characterize the degree of shock metamorphic overprint in meteorites, a variety of different shock classification schemes have been proposed (Haymann 1967; Carter et al. 1968; Van Schmus and Ribbe 1968; Taylor and Heymann 1969; Dodd and Jarosewich 1979; Stöffler et al. 1988, 1991; Scott et al. 1992; Rubin et al. 1997; Schmitt 2000; Sharp and DeCarli 2006; Stöffler and Grieve 2007). Characterizing and quantifying the shock pressure and temperature increase imposed on the meteorite are essential (1) to interpret isotopic measurements related to age dating (Jessberger and Ostertag 1982; Deutsch and Schärer 1994; Fernandes et al. 2009, 2010), (2) in noble gas studies (e.g., Schwenzer et al. 2008), (3) to identify magnetic signatures in planetary or asteroidal rocks (e.g., Weiss et al. 2000; Mang et al. 2013; Reznik

et al. 2016), (4) to know the possibility for organic molecules and life to survive such conditions (e.g., Quirico et al. 2009; Meyer et al. 2011), and (5) to study the collisional history of the planetary system orbiting the Sun (e.g., Beck et al. 2005; Fernandes et al. 2013; Rubin 2015). There is however an ongoing controversy on how to quantify the shock pressure and temperature conditions in the meteorites being studied (Chen et al. 1996; Sharp and DeCarli 2006; Stöffler and Grieve 2007).

The discrepancy between the Stöffler and Grieve (2007) and the Sharp and DeCarli (2006) approaches to determine shock pressures and temperatures in meteorites spawned a discussion about the:

1. Application of dynamic shock versus static high-pressure experimental data to quantify the shock pressure and temperature conditions in naturally shocked rocks (Chen et al. 1996; Sharp and DeCarli 2006; Xie et al. 2006a; Kubo et al. 2010).
2. Formation of diaplectic glasses including maskelynite (Engelhardt et al. 1967; Stöffler et al. 1986; Langenhorst 1994; Chen and El Goresy 2000; Fritz et al. 2005a, 2011a; El Goresy et al. 2013).
3. Influence of shock on the radiometric ages of different isotopic chronometers in different mineral phases (Deutsch and Schärer 1994; Bouvier et al. 2005, 2008; Fritz et al. 2005b; Fernandes et al. 2009, 2013; El Goresy et al. 2013; Moser et al. 2013; Bloch and Ganguly 2014).

Here, the shock classification of meteorites is revisited by recapitulating relevant principles of shock physics, impact cratering, and formation of shock effects in rock-forming minerals. Moreover, the formation and preservation of high-pressure phases in, or near, localized zones of shock melt (veins or pockets) in meteorites is reviewed. Based on this, the contribution aims to reconcile the different views regarding shock-thermo-barometry of meteorites and clarify problems regarding the current shock classification scheme for chondritic meteorites. High-pressure phase assemblages are now identified in a rapidly increasing number of achondritic meteorites, including igneous meteorites from Mars and the Moon (El Goresy et al. 2004; Beck et al. 2005; Fritz and Greshake 2009; Miyahara et al. 2011, 2013; Baziotis et al. 2013; Greshake et al. 2013; Walton 2013; Walton et al. 2014). Therefore, the following discussion on impact physics and shock metamorphism in meteorites is timely and of relevance for various types of stony meteorites.

PHYSICS OF SHOCK METAMORPHISM

A detailed description of shock and impact physics can be found in a variety of publications (Doran and Linde 1966; Melosh 1989; Boslought and Asay 1993; French 1998). A brief summary of some basic knowledge regarding the physics of shock metamorphism focuses on the four key aspects relevant to the aims of this contribution:

1. Shock pressure, temperature, and time constraints in shocked rocks.
2. Cooling history, which depends on the volume of shock-heated material.
3. Evolution of the shape of the shock wave with travel time.
4. Impact velocities and shock pressures inside the isobaric core.

Shock metamorphic effects in meteorites are produced by shock waves. These shock waves are generated during the collision between a smaller projectile and a lager target at velocities exceeding a few km/s, a speed that is significantly higher than the speed at which the impacted material can move out of the way (Melosh 1989; Boslought and Asay 1993). The material is accelerated to a particle velocity slower than the shock front, which travels with a faster shock wave velocity (Fig. 1). The relation between the shock wave and the particle velocity reflects the compressibility of the geo-material at different shock pressures.

During the passage of the shock front through a rock, the particle velocity, pressure, density, temperature, and internal energy increase almost instantly in the involved rocks. The release wave that follows adiabatically unloads the shock compressed material. The impact event accelerates, deforms, and heats the shocked rocks. To understand the petrographic record of this process, it is useful to consider the duration (t) of the dynamically changing pressure (P), and temperature (T) conditions, i.e., P-T-t. An overview of the time intervals in experimentally and naturally shocked rocks is given in Fig. 2 and will be used in the following sections.

Shock Pressure and Temperature

Compared to "normal" crustal metamorphism at pressures of less than a few GPa, the regime of shock metamorphism encompasses much higher pressures of tens to hundreds of GPa that are similar to or even exceed those pressures existing in the Earth's mantle (Fig. 3). Shock metamorphism is characterized by relatively low postshock temperatures of less than 500 °C in nonporous mafic silicate rocks, when shocked below 45 GPa (Figs. 3 and 4). Felsic to mafic rocks shocked to pressures of more than 60 GPa are shock heated to higher temperatures of ≥1200 °C, leading to whole rock melting or vaporization upon decompression.

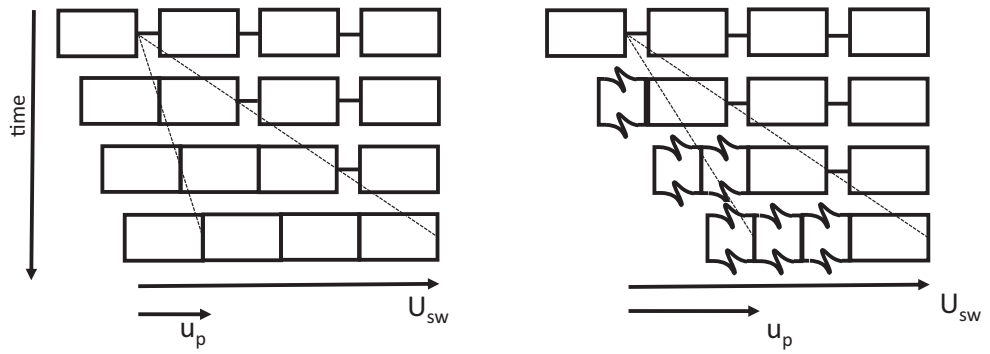

Fig. 1. Illustration of the propagation of the shock wave and the material (particle) for materials of different compressibility. This could be two materials of different compressibility or material shocked to two different pressures at which the compressibility of the material substantially differs. Shock wave velocity = U_{sw}; particle velocity = u_p.

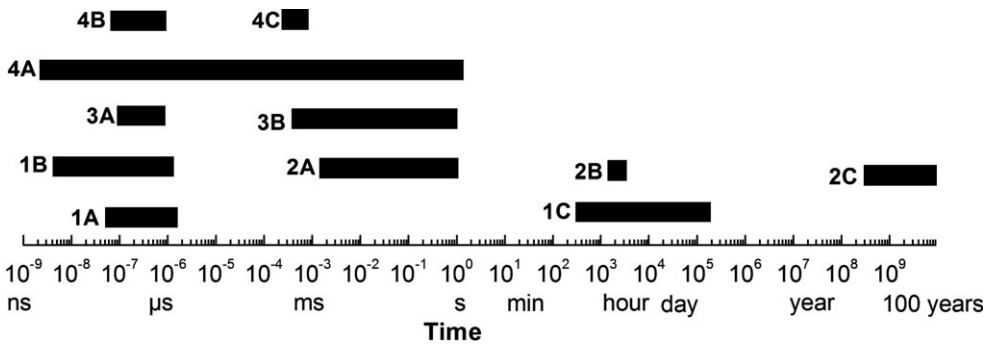

Fig. 2. Overview of the time intervals of shock and thermal effects during impact cratering. Displayed are the duration of shock and static experiments (Langenhorst et al. 2002; Fritz et al. 2011a), shock pulses in rocks during natural impact events and cooling times of millimeter to hundreds of meter sized rock units (Chen et al. 1996; Beck et al. 2005; Fritz et al. 2005b; Xie et al. 2006a, 2006b; Fritz and Greshake 2009). 1A) Free surface velocity measurements of Hugoniot data. 1B) Shock recovery experiments. 1C) Static experiments. 2A) Cooling time of 0.1–1 mm wide shock melt veins. 2B) Cooling time of 0.4–1 m in diameter sized rocks in space. 2C) Cooling time of 10–100 m wide lithologies. 3A) Generation of destructive shock effects. 3B) High pressure phase formation in >10 µm wide melt veins of meteorites. 4A) Shock duration in natural impacts. 4B) Localized shock pressure peaks on the millimeter scale. 4C) Shock pressure equilibration on the meter scale.

The shock-induced temperature increase of the rock to temperatures above its initial state is governed by the pressure-volume work achieved by the shock wave. The calculated postshock temperature increase for different rock types shocked to a range of pressures is shown in Fig. 4. Steepening of the temperature slope for anorthosite, an igneous rock mainly composed of plagioclase, increases at shock pressures higher than those where crystalline plagioclase is transformed into the amorphous maskelynite. Dunite is an igneous rock almost exclusively composed of olivine. Compared to plagioclase, the olivine crystal lattice is more resistant to shock; hence, the steepening of the pressure–temperature curve in dunite occurs at higher shock pressures compared to those for anorthosite (Fig. 4). The differences in compressibility of plagioclase compared to olivine (and also to pyroxene) between 35 and 70 GPa imply that in this pressure range, the shock-induced temperature increase depends strongly on the modal abundance of these minerals within the rock. Another factor that affects the compressibility is the porosity of the rock. Because pore space collapse occurs at pressures <1 GPa, very high shock temperatures can be achieved at low shock pressures in porous rocks (Meyer et al. 2011).

Cooling Times of Shocked Rocks

Above a given shock pressure, the shock-induced modifications will be affected or even completely dominated by thermal effects. The effects of temperature on the petrography of the rock are strongly time-dependent. Thus, in addition to the shock-induced temperature increase, it is important to consider the cooling times, which largely depend on the volume of the shock-heated material. Simplified calculations of the cooling time (t) of a cube of material by thermal conduction are $t = L^2/\alpha$ where L = width of the cube in

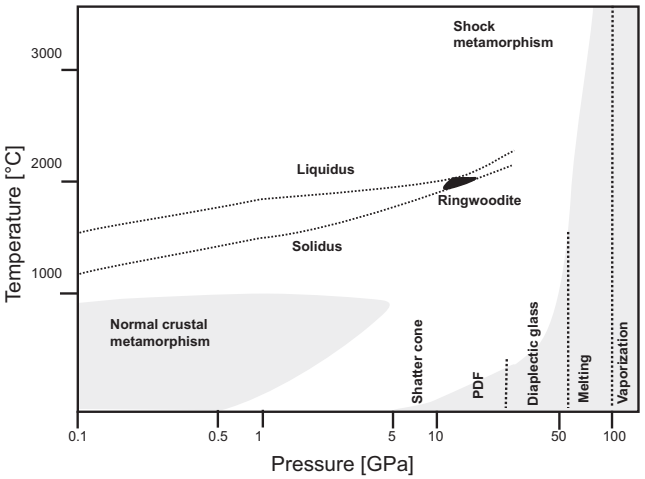

Fig. 3. Pressure versus temperature diagram for regional metamorphism in the Earth's crust compared to shock compression of nonporous silicate rocks (modified after French 1998). The liquidus, solidus, and stability field of ringwoodite, a high-pressure phase of olivine, is displayed as a simplified version of a phase diagram for the composition of the carbonaceous chondrite Allende (Agee et al. 1995). During shock compression, a local temperature excursion in the host rock is required to reach the stability field of ringwoodite.

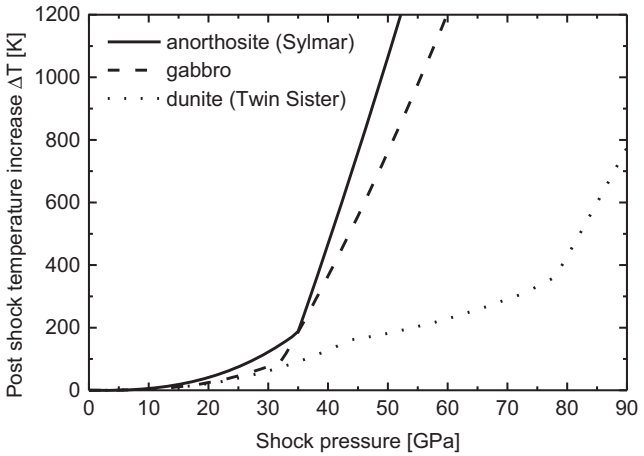

Fig. 4. Postshock temperature increase calculated for different materials using the experimentally measured Hugoniot data of Twin Sister dunite, Sylmar anorthosite (Stöffler 1982), and a gabbro (Trunin et al. 2001). The postshock temperature increase is calculated using the linear relation of shock wave and particle velocity across specific shock pressure intervals as described by Artemieva and Ivanov (2004) and Fritz et al. (2005b). Anorthosite = a felsic igneous rock composed mainly of plagioclase. Gabbro = a mafic plutonic rock composed mostly of plagioclase and pyroxene and sometimes olivine. Dunite = an ultramafic plutonic rock composed mainly of olivine.

meters, and α = thermal diffusivity which in the case of olivine is ~10^{-6} m^2 s^{-1}. Cooling times of a few hundred micrometer wide hot melt veins, in a cold to warm host rock, are on the order of milliseconds (Langenhorst and Poirier 2000; Xie et al. 2006b; Fritz and Greshake 2009). These short cooling times are of relevance for the formation and preservation of high-pressure phases during elevated shock pressure conditions. For comparison, a shock-heated, decimeter diameter sized, rock in space would cool within ten minutes (Fritz et al. 2005a); a time span apparently sufficient to cause a significant loss of radiogenic ^{4}He (Schwenzer et al. 2008), but not sufficient for complete resetting of the ^{40}Ar-^{39}Ar chronometer in strongly shocked rocks containing maskelynite (Fernandes et al. 2009, 2010). Longer cooling times are achieved in larger lithological units in the crater basement or in a warm ejecta blanket (Fernandes and Artemieva 2012) (Fig. 2). Elevated temperatures of years to hundreds of years in ten to hundred meter wide lithologies provide favorable conditions for the degassing of shocked rocks with relevance for their noble gas abundances and ^{40}Ar-^{39}Ar age determinations (Bogard 1995, 2011; Shuster et al. 2010).

Duration of the Shock

The duration of the shock pulse in impact cratering events depends on the size and velocity of the impacting projectile and/or the distance to the nearest "free surface." The free surface is regarded as the interface between the compressed solid material and the atmosphere of the planetary body or the space vacuum. Once the shock front arrives at the surface of the target or the projectile, the high pressure in the rocks cannot be transmitted to the atmosphere or space vacuum. At this free surface, the pressure drops to nearly zero and a pressure release wave is reflected back into the rocks unloading the compressed lithologies (Fig. 5). The pressure release wave gradually overtakes the propagating shock front as it moves at the speed of sound through the compressed and accelerated material. The high particle velocity of the shocked materials does not drop to zero during decompression. After pressure release, the material continues to move with a reduced particle velocity, which drives the excavation flow opening the impact crater.

The duration of the shock for those rocks residing in the base of the target is governed by the size and velocity of the impacting projectile. An example would be the asteroidal meteorites that remained on the parent body after being shocked by an earlier first impact (Chen et al. 1996; Beck et al. 2005; Xie and Sharp 2007) and then ejected from their parent body during a later event. For rocks located at a distance closer to the surface of the target body than the diameter of the

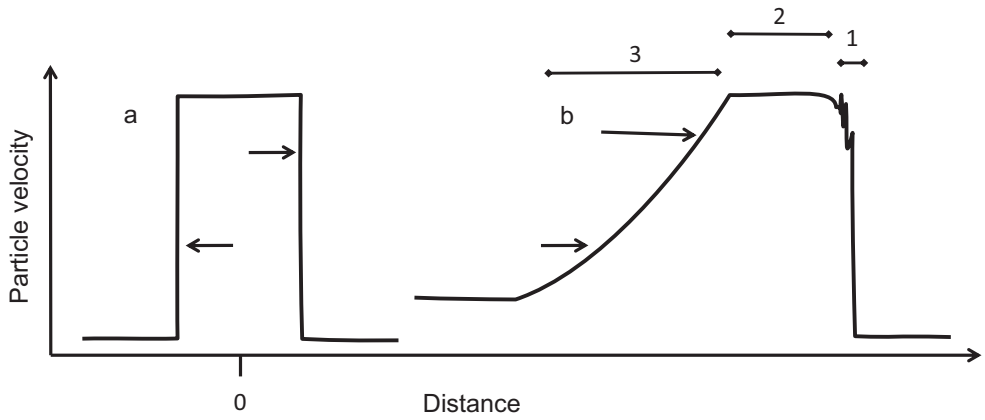

Fig. 5. Propagation of the release wave following a strong shock shown as particle velocity with distance to the plane of impact. The plane of impact is at zero distance. a) Arrows indicate the direction of the shock waves that move from the point of impact into the target and into the projectile. b) Arrows indicate the direction and pressure (length of arrows) of the release wave that was reflected from the back of the projectile (see text: (1) rise of the shock, (2) broad plateau, (3) decompression.

projectile, the shock duration is limited by this preimpact burial depth. For these rocks, the distance to the nearest free surface is shorter than the projectile diameter; hence, the shock duration is significantly shorter. Examples for this case are the Martian and lunar meteorites shocked during their impact ejection into space (Melosh 1984; Fritz and Greshake 2009).

The duration of the shock imposed on the target rock is often on the order of milliseconds (Fig. 2). It may be up to a few seconds for rocks residing at the bottom of a crater in an asteroid during a rare, large, low velocity collision. Notably, the protracted duration of the maximum shock pressure condition is shorter than the time interval of elevated shock pressures. The dynamic rise and fall of the shock pressure in naturally shocked rocks is described in the following two sections.

The Rise of the Shock Front in Polymineralic Rocks

In the ideal case, the shock front presents a sharp discontinuity at which the uncompressed material is directly transferred into a compressed state (Fig. 5a). However on planetary surfaces with lithologies composed of polymineralic rocks, porosity, and cracks with different shock impedances, the shock front is not an ideal discontinuity, instead it can span over a few meters in width (Melosh 1989) (Fig. 5b). This distance of a few meters can be crossed in hundreds of microseconds by a shock wave propagating with a velocity of a few km s^{-1} (Fig. 2). The almost discontinuous increase (jump) in shock pressure at the shock front in polymineralic rocks, and shock pressure equilibration within microseconds, is discussed by Stöffler et al. (1991) and Xie et al. (2006a). For example, at the contact of dense olivine with less dense plagioclase, the particle velocity increases and the pressure decreases. Both particle velocity and pressure have to be the same across the interface between the two materials, thus a release wave is reflected back into the olivine. By comparison, at the contact surface between a less dense olivine and a dense chromite, the particle velocity decreases, the pressure increases, and a pressure wave is reflected back into the olivine grain.

By a series of reflections of a few km s^{-1} fast shock wave, the pressure equilibrates to a general maximum shock pressure. On the scale of a cubic meter of rock (the width of the shock front in planetary surfaces), the pressure equilibration between the mineral grains and pore spaces with different shock impedances occurs within hundreds of microseconds (Fig. 2). Shock and pressure equilibration between pore spaces and minerals of different densities can lead to localized pressure peaks. Pressure peaks localized across submillimeter wide regions, derived from fast shock waves travelling at several km s^{-1}, are short events lasting hundreds of nanoseconds (Fig. 2).

The Shape of the Shock Wave

In contrast to the almost instantaneous pressure rise at the shock front, the rear of the shock wave decays in amplitude because the release wave progressively overtakes the shock front (Fig. 5b). However, the shape of the shock wave is not always characterized by a broad pressure plateau as depicted in Figs. 5a and 5b, but changes with travel time and hence, distance to the point of impact (Figs. 6a–e). As the shock wave propagates forward from the point of impact, the duration of the broad shock pressure plateau decreases, but the maximum shock pressure remains high; i.e., is

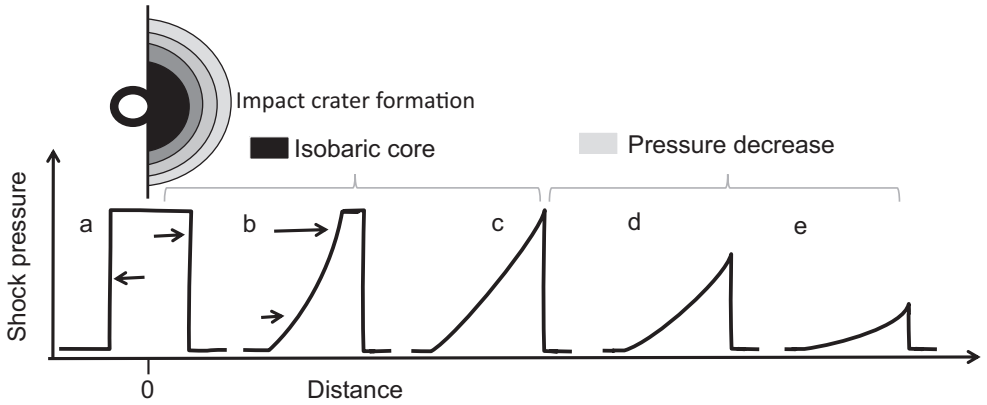

Fig. 6. Pulse length and intensity of a shock wave with distance to the plane of impact. The plane of impact is at zero distance. a) Arrows with different directions show the shock waves that move into the target and into the projectile. b) Arrows with different length show the velocity of the release wave that was reflected from the back of the projectile (see text). The propagating shock wave interacts with the following faster release wave. a–c) In the isobaric core, the shock pressure remains high but the width and, thus, the temporal duration of the broad pressure plateau decreases. d–e) After the shock wave lost the broad pressure plateau, the pressure starts to decrease by interacting with the release wave.

isobaric. The term "isobaric core of an impact cratering event" (from hereon called isobaric core) describes the spatial distribution of material compressed to approximately equal shock pressure. Farther away from the point of impact, the maximum shock pressure starts to decline, because the release wave reaches the shock front.

An important aspect, but neglected in most shock metamorphic studies, is that a shock wave with a broad pressure plateau is restricted to the region inside the isobaric core. Outside the isobaric core, the shock wave has lost its broad pressure plateau, and the maximum shock pressure declines due to interactions with the release wave. The following two sections explain if a shock metamorphic rock could be from within the isobaric core or if it needs to be from a region outside the isobaric core.

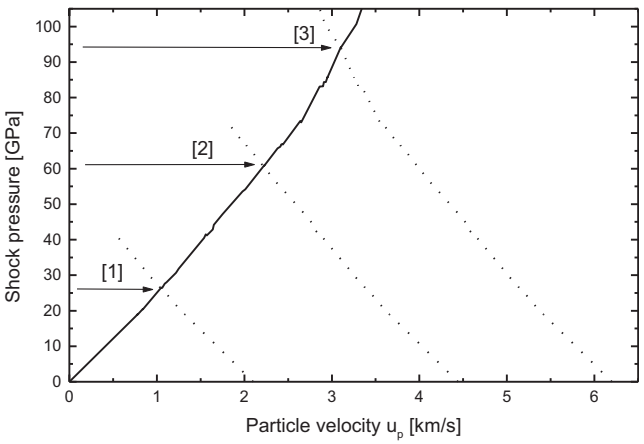

Fig. 7. Graphical determination of the shock pressures produced during planar impacts at different velocities of a projectile and target both made of dunite. The Hugoniot curve for the Twin Sister dunite (data from Stöffler 1982) is displayed as a function of pressure and particle velocity.

Shock Pressures Inside the Isobaric Core

The shock pressure in the isobaric core of an impact cratering event depends on the impact velocity and the types of geo-materials involved. For a given impact velocity and geo-material, the resulting pressures can be graphically derived in the pressure versus particle velocity diagram (Fig. 7). The Hugoniot curve for the target material (solid line) is plotted in the reference frame of the target, i.e., it begins with a pressure and velocity of zero. In this reference frame, the Hugoniot curve for the projectile (dotted lines) is plotted in reverse, i.e., it starts at high impact velocity and zero pressure at the moment before the projectile collides with the target (see Melosh 1989). It is possible to combine Hugoniot data for different types of materials. For simplicity, Fig. 7 shows the impact of a dunitic projectile onto a dunitic target. During impact, the pressure increases in the involved materials and from the viewpoint of the target, the target material is accelerated and the projectile material is decelerated. Across the plane of impact, the materials in the target and the projectile must lie on the Hugoniot curve and have the same particle velocity and pressure. Shock pressures of 26, 60, and 95 GPa are produced in the isobaric core of impacts with velocities of 2.1, 4.5, and 6.2 km s^{-1} (points 1, 2, and 3, respectively, in Fig. 7). This means only low velocity impacts (<4.5 km s^{-1}) allow for shock metamorphism (<60 GPa) inside the isobaric core: the place where isobaric conditions can

prevail for tens to hundreds of milliseconds. In contrast, high velocity impacts >4.5 km s^{-1} induce high shock pressures of >60 GPa inside the isobaric core, causing the target lithologies to melt or vaporize upon decompression.

Typical Impact Velocities onto Asteroids, Mars, Moon, and Earth

Since pressure conditions in the isobaric core are controlled by the impact velocity, it is now possible to discuss whether shock metamorphosed rocks (here restricted to pressures of <60 GPa; see the Shock Pressures Inside the Isobaric Core section) were exposed to a shock wave with a broad pressure plateau. The minimum impact velocity is governed by the escape velocity of the impacted planetary body (in km s^{-1}: Vesta = 0.36; Moon = 2.38; Mars = 5.03; and Earth = 11.2). Excluding secondary cratering and the atmospheric deceleration of small projectiles, the low velocity impacts (<4.5 km s^{-1}) onto the solid surface are restricted to rare cases on asteroids, or the Moon. Notably, the average impact velocity is higher than the escape velocity (in km s^{-1}: Earth = 19.4; Moon = 16.1; Mars = 9.6; and asteroids = 5.8; Farinella and Davis 1992; Ivanov 2001). These simplified considerations of impact velocity and shock pressures inside the isobaric core show that neither Martian nor terrestrial shock metamorphosed rocks were exposed to a shock wave with a broad pressure plateau, the main reason being that the shock pressures inside the isobaric core would melt or vaporize the rock upon decompression. The situation is probably different for chondrites shocked during a rare low velocity (<4.5 km s^{-1}) impact and, hence, low pressure conditions inside the isobaric core, i.e., low enough shock pressures so that the rocks can remain unmelted upon decompression.

GENERATION OF SHOCK METAMORPHIC EFFECTS

Impact conditions such as size and velocity of the impacting bolide influence the properties of the shock wave. The passage of the shock wave through the rock is recorded by two fundamentally different shock-induced modifications. These are the destructive and constructive effects of shock metamorphism reproduced and pressure calibrated by microsecond shock recovery and static pressure experiments, respectively.

Destructive Shock Metamorphic Effects

The destructive shock effects are represented by an increase in disorder of the crystal lattice and material

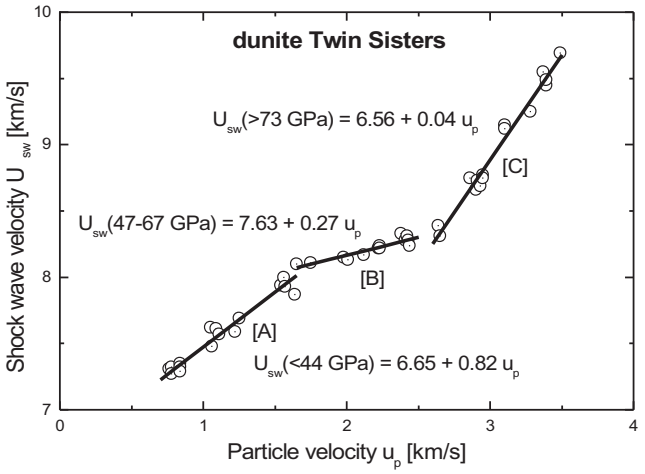

Fig. 8. Experimentally determined shock wave and particle velocity for the Twin Sister dunite as tabulated by Stöffler (1982). The three branches with a linear increase in shock wave and particle velocity are labeled A, B, and C. They reflect substantial changes in the compressibility of the material at these shock pressures. The linear regression given as $U_{sw} = C + S * u_p$ and these C and S values for specific shock pressure intervals can be used to calculate the shock induced temperature increase (see Fig. 4).

volume due to shock compression and decompression. The pressure–volume work in a rock achieved by a shock wave of a given intensity is experimentally quantified by measuring the shock wave and particle velocity (see Figs. 1 and 8). Such data can be found for various geo-materials in Stöffler (1982), Trunin et al. (2001), and in the online database http://teos.ficp.ac.ru/rusbank/. The particle and shock wave velocities at different shock pressures were obtained by measuring the arrival time of the shock wave and the particle velocity at the "free surface" on the back side of the sample (Wackerle 1962). The measured velocities are restricted to a sample layer with a thickness that translates to a pulse length of the shock wave on the order of tens to hundreds of nanoseconds (Fig. 2). The shock wave and particle velocity diagram for the Twin Sister dunite displays three branches labeled A, B, and C in Fig. 8. Each branch shows a linear behavior. Branch A and C would correlate to the situation depicted in Figs. 1a and 1b, respectively. In Fig. 8, the branch A shows that the increase in the shock pressure leads to a linear increase in shock wave and particle velocity. Above a certain pressure, the linear behavior observed for these parameters has a shallower slope (branch B), i.e., a higher increase in the particle velocity. This indicates the start of a physical process where the crystal lattice begins to collapse into a denser phase. The mixed phase region (branch B) persists to pressures at which all the material is compressed to a

denser phase. In the third branch (C), the slope steepens due to a stronger increase in shock wave velocity.

These changes in the shock wave and particle velocity along the branches A, B, and C indicate changes in the properties of the compressed material. Shock recovery experiments with different geo-materials allow the study of the mineralogical effects at well-defined shock pressures by using various methods including macroscopic and microscopic inspection as well as geochemical and spectroscopic analyses (De Carli and Milton 1965; Müller and Hornemann 1969; Snee and Ahrens 1975; Sears et al. 1984; Stöffler et al. 1991; Schmitt 2000; Xie et al. 2001; Fritz et al. 2011a, 2011b). The branch A in the dunite particle and shock wave velocity diagram (Fig. 8) corresponds to pressures at which fractures, dislocations, undulatory extinction, mosaicism, and planar deformation features (PDF) develop in olivine. The "mixed phase region" (branch B) indicates the collapse of the olivine crystal lattice. These pressures correspond to the pressures where brown staining in olivine starts to develop. Brown staining of olivine is caused by Fe-nanoparticles that formed inside the olivine crystals (Van de Moortèle et al. 2007). At higher pressures (branch C), the collapse of the olivine crystal lattice into a denser phase is completed, and brown stained olivine is produced. If shock pressures are further increased, the material will melt or vaporize. These destructive shock effects are (1) a record of the shock wave and particle velocities imposed by the shock, (2) a measure for the pressure-volume work of the shock wave in the material, and (3) directly related to the degree of shock heating. These destructive shock effects develop throughout the entire rock and can be used for whole rock shock-thermo-barometry (see the Shock Pressure and Temperature section). Similar shock effects can be reproduced via different types of shock experiments of 1 ns, 10 ns, and 1 μs duration including pressure pulses by laser irradiation, electric discharge, and high explosive experiments (e.g., Langenhorst et al. 2002) (Fig. 2). Due to their short formation times of less than microseconds, the destructive shock effects record the general maximum shock pressures during shock equilibration (<ms) and the local and short (<μs) pressure spikes.

Constructive Shock Metamorphic Effects

The constructive shock effects are characterized by an increase in lattice order and density of the minerals. The dense high-pressure phases such as ringwoodite, majorite (garnet), bridgmanite (silicate perovskite), and many others form at elevated pressures in, or close to, thin shock melt veins/pockets in meteorites (Binns et al. 1969; Chen et al. 1996, 2003; Tomioka and Fujino 1997; Langenhorst and Poirier 2000; El Goresy et al. 2004; Xie and Sharp 2004, 2007; Miyahara et al. 2008; Fritz and Greshake 2009; Greshake et al. 2013; Tschauner et al. 2014). In these local "hot spots," the high-pressure phases develop through different physical processes including coherent and incoherent solid state transformation processes and crystallization from a melt (Brearley et al. 1992; Kerschhofer et al. 1996, 2000; Liu et al. 1998; Sharp and DeCarli 2006; Fritz and Greshake 2009; Greshake et al. 2013). Most of the high-pressure phases form by kinetically controlled processes requiring very high temperatures (Xie and Sharp 2007). This is because the high-pressure conditions during natural impacts last only a few milliseconds and rarely a few seconds.

Several high-pressure phases provide a maximum temperature value, and by implication, a maximum shock pressure limit for the whole rock. This is because at pressures of zero GPa, the following phases start to decompose in less than seconds, i.e., much faster than the ~30 min cooling time for a 0.4 m diameter meteorite in space (Fritz et al. 2005b) (Fig. 2): (1) bridgmanite (Tschauner et al. 2014) starts to decompose at >130 °C (beginning near 130 °C and completed at 480 °C; Durben and Wolf 1992), (2) akimotoite at >730 °C (Reynard and Rubie 1996), and (3) ringwoodite at >900 °C (Ming et al. 1991; Kimura et al. 2003). In order to preserve these thermally unstable high-pressure phases, the host rock has to serve as a heat sink to allow the thin and hot melt vein/pocket to cool by thermal conduction during a time scale similar to the duration of the shock; i.e., millisecond to second duration (Langenhorst and Poirier 2000; Kimura et al. 2003; Fritz and Greshake 2009).

For example, the preservation of bridgmanite in the Tenham L6 chondrite meteorite (Tschauner et al. 2014) implies postshock temperatures of <130–480 °C. Such low postshock temperatures appear reasonable for nonporous ultramafic rocks (e.g., L6 chondrites with 10 vol% felsic components) shocked to moderate (S4; 15–35 GPa) pressures. For example, a shock-induced temperature increase of 230 °C would raise the temperature of a −100 °C cold rock to an absolute temperature of 130 °C. After decompression to zero GPa, the temperature of the whole rock needs to be lower than the temperature at which high-pressure phases become unstable at low pressure. If not, these thermally unstable high-pressure phases will not be preserved.

SHOCK THERMO-BAROMETRY OF METEORITES

Together with this overview on the generation of the different types of shock metamorphic effects, it is

possible to appreciate the advantages and the inconsistencies of the commonly used approaches for shock thermo-barometry of meteorites. Currently, two different shock classification schemes for chondritic meteorites are in use (Stöffler et al. 1991; Chen et al. 1996; Sharp and DeCarli 2006).

Issues Related to the Current Shock Classification of Meteorites

The current shock classification scheme for ordinary (Stöffler et al. 1991; Stöffler and Grieve 2007), carbonaceous (Scott et al. 1992) and enstatite (Rubin et al. 1997) chondrites progressively assigns shock stages from S1 to S6. Reasonably, the shock classification from S1 to S5 mainly relies on the destructive shock metamorphic effects in the rock-forming minerals that can be observed by optical microscopy. In contrast, the S6 classification explicitly relies on localized effects restricted to regions in, or near, melt zones and not to the shock effects in the whole rock. According to Stöffler et al. (1991), the presence of olivine grains located close to shock melt veins with a characteristic recrystallization texture is the prime criterion for shock stage S6, and ringwoodite may be present. Rubin et al. (1997) further suggested that, in the case of enstatite chondrites, the presence of the high-pressure phase majorite is characteristic for S6 rocks. To date, this type of shock classification scheme has not been applied to achondritic meteorites. However, as high-pressure phases are recognized in an ever increasing number of achondritic meteorites (e.g., Lipschutz 1964; El Goresy et al. 2004; Fritz and Greshake 2009; Walton et al. 2014; Miyahara et al. 2016), it is timely to revisit the current reasoning and praxis of using the shock classification of chondrites and its implications for the shock pressure barometry of stony meteorites in general.

The shock classification of meteorites aims to describe the shock pressure and temperature conditions of the whole rock. As mentioned previously, the diagnostic properties of the S6 classification explicitly rely on localized phenomena in or near melt zones (Stöffler et al. 1991; Stöffler and Grieve 2007). This leads to a problematic situation for the following reasons:

1. The main criteria for S6 is the recrystallization of olivine in and around a melt vein/pocket. This spatial restriction implies that the amount of heat required for driving the recrystallization came from within these local "hot spots." However, the amount of heat or the volumetric dimension of a hot melt zone is not a diagnostic criterion for very high shock pressures in the whole rock. Actually, the presence of melt veins is not even a distinguishing mark for shock, as it could be due to friction only. Thus, the localized recrystallization of olivine cannot be considered a diagnostic criterion to describe the shock pressure and temperature conditions in the whole rock.
2. The mineral ringwoodite displays a blue to green color in transmitted light (Taran et al. 2009), and in many L6 chondrites especially, it can be easily recognized by optical microscopy (Fig. 9). Presently, it is common practice to use the presence of ringwoodite as a prime criterion for the S6 shock classification. However, the S6 classification combines high temperatures of 850–1750 °C with the possible presence of mafic high-pressure phases such as ringwoodite. These two criteria exclude each other as several high-pressure phases are unstable at that high temperatures and pressures of zero GPa.

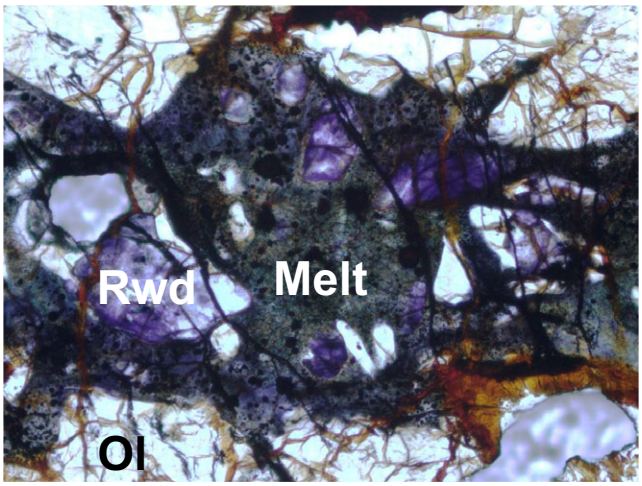

Fig. 9. Transmitted light optical microscope image of pink to greenish ringwoodite in the melt vein of the L6 chondrite Northwest Africa 6525. Field of view is 400 μm wide. Rwd = ringwoodite; Ol = olivine. (Color figure can be viewed at wileyonlinelibrary.com.)

Formation of Isobaric High-Pressure Phase Assemblages

As mentioned in the Issues Related to the Current Shock Classification of Meteorites section, the shock pressures inferred from high-pressure phases are significantly lower than those concluded from the S6 shock classification, and slightly to moderately lower than the shock pressures deduced from the shock effects in the main rock-forming minerals. The latter observation will be addressed below.

The use of high-pressure phases to determine the shock pressures in a rock relies on the assumption that the shock wave had a broad pressure plateau that

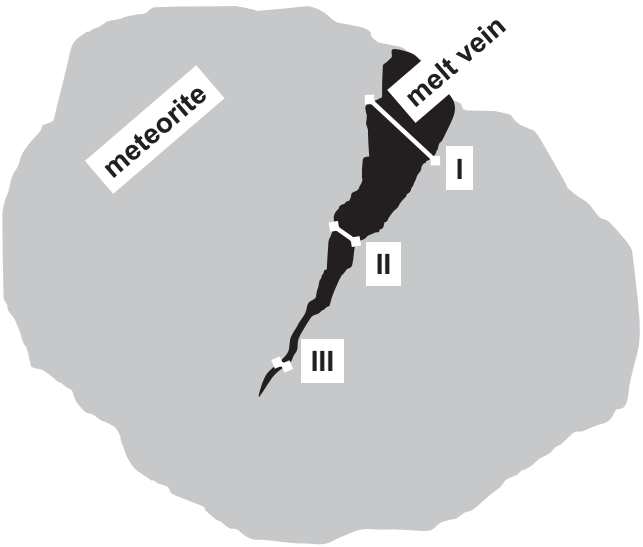

Fig. 10. Sketch of a meteorite hosting a melt vein with different thickness. Depending on the size of the melt, it quenches at time scales (I) longer, (II) equal to, or (III) shorter than the duration of the shock. This means the melt vein quenches in situation (I) after pressure release, in situation (II) during pressure release, and in situation (III) at isobaric conditions if the host rock is within the isobaric core or during declining shock pressure if the rock is outside the isobaric core.

lasted for milliseconds to seconds (see figs. 5a, 5b, and 7 in Xie et al. [2006a] or fig. 15 in Sharp and DeCarli [2006]). Hence, it would be expected that a melt vein of appropriate size quenches at isobaric pressures during this time span (Fig. 10). Chen et al. (1996) and Sharp and DeCarli (2006) therefore concluded that isobaric high-pressure phase assemblages in shock melt zones in meteorites can, and should, be used as a shock-barometer for the pressure conditions in the whole rock.

Here, it is argued that high-pressure phases observed in melt veins/pockets of meteorites record lower pressure, at a later time, than those recorded by the destructive shock effects. A shock wave with a broad pressure plateau is restricted to the region inside the isobaric core (see The Shape of the Shock Wave section). For impacts in the inner solar system including the asteroid belt with typical impact velocities of >5.8 km s^{-1} (see the Shock Pressures Inside the Isobaric Core and Typical Impact Velocities onto Asteroids, Mars, Moon and Earth sections), the resulting pressures in the isobaric core would cause the involved lithologies to melt and/or vaporize upon decompression. This means that shock metamorphosed rocks (<60 GPa) from impact events faster than 5 km s^{-1} were located outside the isobaric core. Note that a collision speed limit for impact events with an isobaric core of 16–23 GPa, the pressures value for the stability field of ringwoodite, is around 2 km s^{-1}.

A COMPARISON OF IMPACT CONDITIONS AND SHOCK METAMORPHISM IN METEORITES FROM DIFFERENT PARENT BODIES

To illustrate the conclusion, three specific cases will be briefly compared. (1) For Martian meteorites, the minimum impact velocity onto Mars (5.3 km s^{-1}) is too high to allow for shock metamorphism inside the isobaric core, i.e., the rocks would melt or vaporize; (2) for H; and (3) for L type ordinary chondrites, the minimum impact velocity onto asteroids is <0.4 km s^{-1} and the average impact velocity is ~5.8 km s^{-1}. The values for the minimum impact velocity means that for the L and H chondritic meteorites, it is theoretically possible that the pressures in the isobaric core are low enough for shock metamorphism. The values for the average impact velocity on asteroids means that most of the impact events occurred at velocities >4.5 km s^{-1} resulting in too high shock pressures inside the isobaric core for rocks to remain solid.

Ringwoodite, the high-pressure polymorph of olivine, has so far been found in the Martian meteorites Chassigny (Fritz and Greshake 2009), Elephant Moraine 79001 (Walton 2013), Dar al Gani 670 (Greshake et al. 2013) and Tissint (Baziotis et al. 2013; Walton et al. 2014). When comparing these meteorites, they also display substantial differences in shock effects in olivine ranging from undulatory extinction in Chassigny to strong mosaicism in Dar al Gani 670. In Chassigny, ringwoodite is found conjoined with wadsleyite (a high-pressure phase of olivine stable at pressures lower than ringwoodite) and the high-pressure decomposition products of olivine such as ferropericlase (Mg,Fe[O]). Both findings convincingly suggest that in Martian meteorites, the high-pressure phase assemblages formed during shock pressure decline. Consequently, for this Martian meteorites, the high-pressure phase assemblages observed cannot be used to deduce the general maximum shock pressure of the rock, as the derived values would be too low.

High-pressure phase assemblages in ordinary chondrites are very prominent in L6 chondrites and significantly less abundant in H chondrites (e.g., Binns et al. 1969; Xie et al. 2001). H chondrites display a range of impact ages older than 3.6 Ga and various impact ages younger than 1.3 Ga (Swindle et al. 2009; Bogard 2011). Consequently, H chondrites record a variety of impacts (Wittmann et al. 2010), with a collision velocity distribution that should be typical for the asteroid belt (~5.8 km s^{-1} on average; Farinella and Davis 1992). The striking differences between shock

melt veins in H and L chondrites might be explained by an unusually large impact onto the L chondrite parent body.

A large number of L chondrites experienced radiometric age resetting at ~480 Ma ago (Haymann 1967; Bogard 1995; Korochantseva et al. 2007). This thermally induced age resetting is apparently related to a major disruption event of the L chondrite parent body at that time which is coincident with a large number of fossil meteorites recovered from mid Ordovician limestones (Schmitz et al. 2001). Thus, high-pressure phases in L6 chondrites may reasonably reflect the conditions during one extraordinary impact event (Chen et al. 1996; Xie et al. 2006a, 2006b). Hence, these conditions cannot be constrained by statistical arguments based on the average impact velocity in the asteroid belt. Notably, Xie et al. (2006a) investigated the high-pressure phases in melt veins of the L6 Tenham meteorite, and concluded that the sample experienced a peak-shock pressure of 25 GPa near the point of impact, which occurred at ~2 km s^{-1}. Such a scenario of isobaric high-pressure phase assemblages being restricted to samples close to the point of a low velocity impact would be theoretically possible. Comparing the range of shock metamorphism recorded by the L chondrites shocked during this impact event at ~480 Ma ago may aid in constraining the impact conditions.

Nevertheless, low velocity impacts that instead of melting or vaporization, allow for shock metamorphism inside an isobaric core are rather the exception than the norm. Therefore, a general shock classification of extraterrestrial rocks cannot rely on high-pressure phase assemblages in or near shock melt pockets and veins. The presence of ringwoodite in many Martian meteorites, together with a minimum impact velocity on Mars of 5.3 km s^{-1}, demonstrates that high-pressure phase assemblages can quickly form in local hot spots during shock pressure decline.

SUGGESTED MODIFICATIONS FOR THE SHOCK PRESSURE CLASSIFICATION SCHEME

The current practice of using the localized occurrence of ringwoodite and other mafic high-pressure phases as diagnostic for the S6 shock classification of chondrites results in an overestimation of the shock pressure and temperature conditions in the whole rock. Adopting such logic for other types of stony meteorites would lead to incorrect results in all types of shocked rocks. Based on the arguments presented in the previous sections, a revised shock pressure classification scheme is proposed (Table 1). Each type of high-pressure phase in or near melt veins and pockets provides a minimum value for the general maximum shock pressure to allow the formation of this phase, and a maximum postshock temperature of the whole rock after decompression to allow the preservation of this phase. High-pressure phases that are unstable at pressures of zero GPa and elevated temperatures are absent in very highly shocked rocks (S6). S6 rocks are characterized by brown stained olivine and shock melted plagioclase in the whole rock.

Localized recrystallization of olivine proposed as the prime criteria for S6 rocks (Stöffler et al. 1991) can occur in very strongly shocked rocks with high whole rock temperatures. Nevertheless, thermal phenomena restricted to small regions, in or attached to localized melt zones, such as the recrystallization of olivine, are not a relevant criteria for determining the shock pressure and temperature conditions of the whole rock. Notably, the formation of melt veins can occur by different processes and, thus, does not present direct evidence for a shock. Bleaching of brown stained olivine around local melt zones can be used as a criterion for S6 if shock staining of olivine occurs throughout the whole meteorite.

In strongly (S5) to very strongly (S6) shocked rocks, (Table 1) some shock metamorphic effects are altered or fully replaced by thermal overprinting due to high postshock temperatures and long cooling times. For rocks shocked to high pressures in the S5 to S6 range, the shock-induced temperature increase strongly depends not only on porosity but also on the mineralogical composition of the rock (see the Shock Pressure and Temperature section). In addition, the effects of temperature on the petrography of the rock are strongly time-dependent. High temperatures of 600 °C may not result in annealing of shock metamorphic effects of ejected decimeter scale rock fragments that cool in less than one hour. However, the same temperature may change the petrography of rocks that remain at elevated temperatures for years to hundreds of years buried in the crater basement (Rubin 2004). Clearly, the intensity of the thermal overprint on the shock effects strongly depends on several factors, including rock mineral composition and time, which are not a measure for the degree of shock pressure.

Consequently, for the purpose of shock classification, the diagnostic criteria should be restricted to shock effects sensu stricto: The shock effects observed in minerals outside the melt veins/pockets should be representative for the main mass of the rock as they are used to describe the shock conditions in the whole meteorite. The diagnostic criteria for S6 include olivine with strong mosaicism, in part smoothed by recrystallization and shock-induced brown staining, a feature which is not affected by mild annealing. The

Table 1. Revision of the shock classification scheme for olivine-rich crystalline rocks including chondrites initially proposed by Stöffler et al. (1991) and Stöffler and Grieve (2007). The occurrence of high-pressure phases requires shock pressures equal to, or higher than, indicated by their stability field, and postshock temperatures in the whole rock that are lower than the threshold temperature for their back reaction a pressures of zero GPa. In practice, the occurrence of high-pressure phase assemblages (constructive shock effects) is restricted to "hot spots" of localized shock melt. Localized shock melt and, hence, the constructive shock effects appear in rocks of at least shock stage S3. Back reaction temperatures for ringwoodite are from Ming et al. (1991) and for bridgmanite from Durben and Wolf (1992). Shock pressures required to transform plagioclase with different chemical composition into maskelynite can be found in Stöffler et al. (1986), Schmitt (2000), Johnson and Hörz (2003), and Fritz et al. (2011b). Note that increasing the shock pressure eventually leads to whole rock melting, but a variety of processes can lead to melting of rocks. Melted rocks are not a unique shock feature and, thus, not part of the shock classification scheme.

			Destructive shock effects in rock-forming minerals		Mineralogy of localized polymineralic melt zones including constructive shock effects
Shock stage	*P* (GPa)	*T* (°C) (postshock)	Olivine	Plagioclase	
S1					
Unshocked	<4–5	10–20	Sharp optical extinction with <2° angular variation	Sharp optical extinction (for chemically unzoned plagioclase)	
S2					
Very weakly shocked	5–10	20–50	Undulatory extinction with >2°angular variation	Undulatory extinction	
S3					
Weakly shocked	15–20	100–150	Undulatory extinction, Planar fractures (PF)	Undulatory extinction	Glass, low pressure (LP), and possibly high-pressure (HP) minerals such as Wadsleyite (Wds), ringwoodite (Rwd), majorite (Maj)
S4					
Moderately shocked	25–35	200–300	Weak mosaicism and PF	Low grade: undulatory extinction; High grade: partially isotropic, PDF	Glass, LP, and possibly HP minerals such as Wds, Rwd, Maj, bridgmanite (Bdm), ferropericlase (Fpc)
S5					
Strongly shocked	45–60	600–900	Strong mosaicism, planar deformation features (PDF) and PF	Maskelynite; Note: minimum pressure for maskelynitization (20–35 GPa) falls with rising Ca-content	Glass, LP, and possibly HP minerals such as Wds, Rwd, Maj, Fpc; back reaction of bdm
S6					
Very strongly shocked		1500–1700	Strong mosaicism, PDF, recrystallization, brown staining	Shock melted glass with flow structures, vesicles and fusing of adjacent minerals; recrystallization	Glass, devitrified glass, LP minerals; bleaching of brown stained olivine, recrystallization
Shock melted	Whole rock melting and formation of melt rock				

shock-induced brown staining of olivine can subsequently be bleached by intense thermal metamorphism near local zones of hot shock melt. Melting of plagioclase is indicated by flow structures, vesiculation, and/or eutectic melting at the contact of plagioclase to pyroxene. Destructive shock effects in other minerals diagnostic for shock pressures in excess of 45–60 GPa can be added to the list of diagnostic shock features. A likely example for an S6 achondrite using these criteria is the Martian meteorite Allan Hills 77005 displaying an intense shock metamorphic overprint of the rock-forming minerals including brown staining of olivine, vesiculated plagioclase glass that partly recrystallized at postshock temperatures of ~1000 °C, and localized recrystallization and bleaching of the brown stained olivine (Fritz et al. 2005b). Despite a thorough search, no high-pressure phases were identified in this meteorite (El Goresy et al. 2013).

Using the destructive shock effects for a general classification appears essential because the destructive shock effects:

1. Are the physical manifestation of the pressure-volume work achieved by the shock wave upon the target material, and as a result, are physically related to the shock-induced temperature increase.
2. Can be observed by optical microscopy, allowing for shock classification of thin sections in a reasonable amount of time.
3. Allow the classification of weakly to very strongly shocked rocks. Both the weakly and the very strongly shocked rocks are, for different reasons, characterized by the absence of high-pressure phases.
4. Can form on time scales of less than microseconds when each part of the mineral grain can record its maximum pressure. The general maximum shock pressure in the whole rock is recorded by the average degree of shock deformations displayed by the major rock-forming minerals constituting the main mass of the meteorite.
5. Quickly record the highest shock pressures, whereas the high-pressure phases need some time to form and thus, mostly reflect the conditions during the decline of the shock pressure.

SUMMARY

This work provides an overview on the physics of impact cratering and the mineralogy of shock metamorphism. The aim is to address the controversies in the shock thermo-barometry and shock classification of meteorites (Stöffler et al. 1991; Chen et al. 1996; Sharp and DeCarli 2006).

Meteorites record shock metamorphic effects due to shock pulses with durations ranging between nanoseconds and seconds. This includes localized and therefore short (<μs) pressure spikes, which may lead to the localized formation of shock melt. Shock pressure equilibration between the different minerals within a cubic meter rock occurs within milliseconds. This general maximum shock pressure (sometimes called the equilibration shock pressure) is recorded by the destructive shock effects in those rock-forming minerals that constitute the main mass of the rock. Shock melt veins are small local "hot spots" and some have a specific size that allows for rapid cooling by thermal conduction in very short time scales similar to the duration of the shock. These local melt zones can host high-pressure phase assemblages that formed at elevated shock pressure, i.e., the constructive shock metamorphic effects.

Here, it is emphasized the relation between impact velocity, shock pressures in the isobaric core, and the evolution of the shape of the shock wave as it propagates away from the point of impact. This means that, in most cases, a shock metamorphic rock did not experience a shock wave with a broad pressure plateau of millisecond duration. Instead, it experienced a shock wave with continuously declining in pressure due to overtaking by the release wave. This is of fundamental relevance to understand that the destructive shock effects observed in the rock-forming minerals are indicative of higher pressures than those deduced from the high-pressure phase assemblages in melt zones of meteorites.

So far, most researchers assume that the difference between these two barometers, i.e., the destructive and the constructive shock effects, in meteorites means that one of them does not provide reliable results. This is the logical outcome when considering cooling times of melt veins jointly with the assumption that the shock wave has a broad pressure plateau; i.e., the melt veins of appropriate size have to be quenched during isobaric conditions.

Here, it is argued that in most cases the shock wave does not have a broad pressure plateau (>ms). As a result, the melt veins did not quench during isobaric pressure conditions. Thus, the two mineral shock barometers, (1) the destructive shock effects calibrated by microseconds shock experiments, and (2) the high-pressure phase assemblages as calibrated by static experiments, both provide reliable results. In all types of meteorites, these two barometers record different pressures at different times. Therefore, they bear information on the changes of the shock pressure in the whole rock with time, and the temperature that equilibrates between the hot melt vein and the cooler host rock. The shock metamorphic record can be used to infer the shape of the shock wave and the impact conditions on the parent body.

The established shock classification scheme for meteorites needs to be updated. This is because the S6 classification explicitly relies on localized effect restricted to regions in or near melt zones, and not on the properties of the whole rock. The localized recrystallization of olivine depends on the amount of heat in the melt zone and not on the pressure and temperature conditions in the whole rock.

Most importantly, the established classification schemes for ordinary, enstatite, and carbonatious chondrites (Stöffler et al. 1991; Scott et al. 1992; Rubin et al. 1997) are understood such that mafic high-pressure phases are diagnostic for very highly shocked rocks (S6). This shock classification does not consider that many mafic high-pressure phases, such as ringwoodite or bridgmanite, are unstable at elevated temperatures and pressures of zero GPa. This means these phases cannot survive the high temperatures in

very strongly shocked rocks after decompression. The current usage of the shock classification scheme results in significantly overestimated shock pressure and temperature conditions for all meteorites hosting mafic high-pressure phase assemblages. Because high-pressure phase assemblages have now been identified in a variety of different meteorite types, this reasoning is of relevance not only for chondritic meteorites, but also for other achondritic silicate rocks.

CONCLUSION

It is here proposed an update for the S6 classification that purely relies on the destructive shock effects in the rock-forming minerals as a measure for the shock pressures affecting the whole rock. Brown staining of olivine and shock melting of plagioclase are characteristic properties of these very highly shocked rocks (S6).

Most, to all, rocks currently classified as S6 are likely to have an incorrect shock classification. This is because neither of the criteria, the localized recrystallization of olivine and the presence of ringwoodite, provide a reliable measure for very high shock pressures.

The destructive shock effects in the rock-forming minerals record the general maximum shock pressure in the whole rock. The constructive shock deformation effects in and near local hot spots allows investigation on the duration of the shock and the shape of the shock wave. The combination of destructive and constructive shock metamorphic effects allows us to reconstruct the shock pressure-temperature-time conditions in shocked meteorites. This has implications for the size and velocity of the impacting bolide and the location of the rock during the impact process. Shock metamorphic research thus opens a window to impact processes and the collisional history of the planetary system revolving around Sun.

Acknowledgments—Financial support for JF by *Saalbau goes Science* and VAF through the DFG research grant FE 1523/3-1. This work made use of the NASA ADS abstract service. We are grateful for the helpful review from an anonymous reviewer. Stephen Edwards is thanked for proofreading and further commenting, which greatly improved the manuscript.

Editorial Handling—Dr. A. J. Timothy Jull

REFERENCES

Agee C. B., Li J., Shannon M. C., and Circone S. 1995. Pressure temperature phase diagram for the Allende meteorite. *Journal of Geophysical Research* 100:725–740.

Artemieva N. A. and Ivanov B. 2004. Launch of Martian meteorites in oblique impacts. *Icarus* 171:84–101.

Baziotis I. P., Yang L., DeCarli P. S., Melosh H. J., McSween H. Y., Bodnar R. J., and Taylor L. A. 2013. The Tissint Martian meteorite as evidence for the largest impact excavation. *Nature Communications* 4:1404. doi:10.1038/ncomms2414.

Beck P., Gillet P., El Goresy A., and Mostefaoui S. 2005. Timescales of shock processes in chondritic and Martian meteorites. *Nature* 435:1071–1074.

Binns R. A., Davis R. J., and Reed S. J. B. 1969. Ringwoodite, natural $(Mg, Fe)_2SiO_4$ spinel in the Tenham meteorite. *Nature* 221:943–944.

Bloch E. and Ganguly J. 2014. ^{176}Lu-^{176}Hf and ^{147}Sm-^{143}Nd ages of the Martian shergottites: Evaluation of the shock-resetting hypothesis through diffusion kinetic experiments and modeling, and petrological observations. *Earth and Planetary Science Letters* 395:173–183.

Bogard D. D. 1995. Impact ages of meteorites: A synthesis. *Meteoritics & Planetary Science* 30:244–268.

Bogard D. D. 2011. K-Ar ages of meteorites: Clues to parent-body thermal histories. *Chemie der Erde* 71:207–226.

Boslough M. B. and Asay J. R. 1993. Basic principles of shock compression. In *High-pressure shock compression of solids*, edited by Asay J. R. and Shanhinpoor M. New York: Springer. 393 p.

Bouvier A., Blichert-Toft J., Vervoort J. D., and Albaréde F. 2005. The age of SNC meteorites and the antiquity of the Martian surface. *Earth and Planetary Science Letters* 240:221–233.

Bouvier A., Blichert-Toft J., Vervoort J. D., Gillet P., and Albarède F. 2008. The case for old basaltic shergottites. *Earth and Planetary Science Letters* 266: 105–124.

Brearley A. J., Rubie D. C., and Ito E. 1992. Mechanisms of the transformations between the α-polymorphs, β-polymorphs and γ-polymorphs of Mg_2SiO_4 at 15 GPa. *Physics and Chemistry of Minerals* 18:343–358.

Carter N. L., Raleigh C. B., and DeCarli P. S. 1968. Deformation of olivine in stony meteorites. *Journal of Geophysical Research* 73:5439.

Chen M. and El Goresy A. 2000. The nature of maskelynite in shocked meteorites: Not a diaplectic glass but a glass quenched from shock-induced dense melt at high pressures. *Earth and Planetary Science Letters* 179:489–502.

Chen M., Sharp T. G., El Goresy A., Wopenka B., and Xie X. 1996. The majorite pyrope magnesiowustite assemblage: Constraints on the history of shock veins in chondrites. *Science* 271:1570–1573.

Chen M., Shu J. F., Xie X. D., and Mao H. K. 2003. Natural $CaTi_2O_4$-structured $FeCr_2O_4$ polymorph in the Suizhou meteorite and its significance in mantle mineralogy. *Geochimica et Cosmochimica Acta* 67:3937–3942.

De Carli P. S. and Milton D. J. 1965. Stishovite: Synthesis by shock wave. *Science* 147:144–145.

Deutsch A. and Schärer U. 1994. Dating terrestrial impact events. *Meteoritics* 29:301–322.

Dodd R. T. and Jarosewich E. 1979. Incipient melting in and shock classification of L-group chondrites. *Earth and Planetary Science Letters* 44:335–340.

Doran D. G. and Linde R. K. 1966. Shock effects in solids. In *Solid state physics*, edited by Seitz F. and Turnbull D. Amsterdam: Elsevier. pp. 229–290.

Durben D. J. and Wolf G. H. 1992. High-temperature behavior of metastable $MgSiO_3$ perovskite: A Raman spectroscopic study. *American Mineralogist* 77:890–893.

El Goresy A., Dubrovinsky L., Sharp T. G., and Chen M. 2004. Stishovite and post-stishovite polymorphs of silica in the shergotty meteorite: Their nature, petrographic settings versus theoretical predictions and relevance to Earth's mantle. *Journal of Physics and Chemistry of Solids* 65:1597–1608.

El Goresy A., Gillet P., Miyahara M., Ohtani E., Ozawa S., Beck P., and Montagnac G. 2013. Shock-induced deformation of Shergottites: Shock-pressures and perturbations of magmatic ages on Mars. *Geochimica et Cosmochimica Acta* 101:233–262.

Engelhardt W. von, Arndt J., Stöffler D., Müller W. F., Jeziorkowski H., and Gubser R. A. 1967. Diaplektische Gläser in den Breccien des Ries von Nördlingen als Anzeichen für Stoßwellenmetamorphose. *Contributions to Mineralogy and Petrology* 15:93–102.

Farinella P. and Davis D. R. 1992. Collision rates and impact velocities in the main asteroid belt. *Icarus* 97:111–123.

Fernandes V. A. and Artemieva N. 2012. Impact ejecta temperature profile on the Moon—What are the effects on the Ar-Ar dating method? (abstract #1367). *43rd Lunar and Planetary Science* Conference. CD-ROM.

Fernandes V. A., Burgess R., and Morris A. 2009. ^{40}Ar-^{39}Ar age determinations of lunar basalt meteorites Asuka 881757, Yamato 793169, Miller Range 05035, LaPaz Icefield 02205, Northwest Africa 479, and basaltic breccia Elephant Moraine 96008. *Meteoritics & Planetary Science* 44:805–821.

Fernandes V. A., Fritz J., Wünnemann K., and Hornemann U. 2010. Lunar meteorites: Shock effects vs. ^{40}Ar-^{39}Ar age (abstract). The Ries crater, the Moon, and the future of human space exploration, Nördlingen, Germany. p. 11.

Fernandes V. A., Fritz J., Weiss B. P., Garrick-Bethell I., and Shuster D. L. 2013. The bombardment history of the Moon as recorded by ^{40}Ar-^{39}Ar chronology. *Meteoritics & Planetary Science* 48:241–269.

French B. M. 1998. Traces of catastrophe: A handbook of shock-metamorphic effects in terrestrial meteorite impact structure. Technical Report, LPI-Contribution 954. Houston, Texas: Lunar and Planetary Institute. 120 p.

Fritz J. and Greshake A. 2009. High pressure phases in an ultramafic rock from Mars. *Earth and Planetary Science Letters* 288:619–623.

Fritz J., Greshake A., and Stöffler D. 2005a. Micro-Raman spectroscopy of plagioclase and maskelynite in Martian meteorites: Evidence of progressive shock metamorphism. *Antarctic Meteorite Research* 18:96–116.

Fritz J., Artemieva N. A., and Greshake A. 2005b. Ejection of Martian meteorites. *Meteoritics & Planetary Science* 40:1393–1411.

Fritz J., Wünnemann K., Reimold W. U., Meyer C., and Hornemann U. 2011a. Shock experiments on quartz targets pre-cooled to 77 K. *International Journal of Impact Engineering* 38:440–445.

Fritz J., Wünnemann K., Greshake A., Fernandes V. A. S. M., Boettger U., and Hornemann U. 2011b. Shock pressure calibration for lunar plagioclase (abstract #1196). 42nd Lunar and Planetary Science Conference. CD-ROM.

Fritz J., Bitsch B., Kührt E., Morbidelli A., Tornow C., Wünnemann K., Fernandes V. A., Grenfell J. L., Rauer H., Wagner R., and Werner S. C. 2014. Earth-like habitats in planetary systems. *Planetary and Space Science* 98:254–267.

Greshake A., Fritz J., Böttger U., and Goran D. 2013. Shear-induced ringwoodite formation in the Martian shergottite Dar al Gani 670. *Earth and Planetary Science Letters* 375:383–394.

Haymann D. 1967. On the origin of hypersthene chondrites: Ages and shock effects of black chondrites. *Icarus* 6:189–221.

Ivanov B. A. 2001. Mars/Moon cratering rate ratio estimates. *Space Science Reviews* 96:87–104.

Jessberger E. K. and Ostertag R. 1982. Shock-effects on the K-Ar system of plagioclase feldspar and the age of anorthosite inclusions from North-Eastern Minnesota. *Geochimica et Cosmocimica Acta* 46:1465–1471.

Johnson J. R. and Hörz F. 2003. Visible/near-infrared spectra of experimentally shocked plagioclase feldspars. *Journal of Geophysical Research (Planets)* 108k:6–1.

Kerschhofer L., Sharp T. G., and Rubie D. C. 1996. Intracrystalline transformation of olivine to wadsleyite and ringwoodite under subduction zone conditions. *Science* 274:79–81.

Kerschhofer L., Rubie D. C., Sharp T. G., McConnell J. D. C., and Dupas-Bruzek C. 2000. Kinetics of intra-crystalline olivine ringwoodite transformation. *Physics of Earth and Planetary Interior* 121:59–76.

Kimura M., Chen M., Yoshida Y., El Goresy A., and Ohtani E. 2003. Back-transformation of high-pressure phases in a shock melt vein of an H-chondrite during atmospheric passage: Implications for the survival of high-pressure phases after decompression. *Earth and Planetary Science Letters* 217:141–150.

Korochantseva E. V., Trieloff M., Buikin A. I., Lorenz C. A., Ivanova M. A., Schwarz W. H., Hopp J., and Jessberger E. K. 2007. Chondrite asteroid breakup tied to Ordovician meteorite shower by multiple isochron ^{40}Ar-^{39}Ar dating. *Meteoritics & Planetary Science* 42:113–130.

Kubo T., Kimura M., Kato T., Nishi M., Tominaga A., Kikegawa T., and Funakoshi K.-I. 2010. Plagioclase breakdown as an indicator for shock conditions of meteorites. *Nature Geoscience* 3:41–45.

Langenhorst F. 1994. Shock experiments on pre-heated α- and β-quartz: II. X-ray and TEM investigations. *Earth and Planetary Science Letters* 128:683–698.

Langenhorst F. and Poirier J. P. 2000. Anatomy of black veins in Zagami: Clues to the formation of high-pressure phases. *Earth and Planetary Science Letters* 184:37–55.

Langenhorst F., Boustie M., Deutsch A., Hornemann U., Matignon C., Migault A., and Romain J. P. 2002. Experimental techniques for the simulation of shock metamorphism: A case study on calcite. In *High-pressure shock compression of solids V–Shock chemistry with applications to meteorite impacts*, edited by Davison L., Horie Y., and Sekine T. New York: Springer. pp. 1–27.

Lipschutz M. E. 1964. Origin of diamonds in the Ureilites. *Science* 143:1431–1434.

Liu M., Kerschhofer L., Mosenfelder J., and Rubie D. C. 1998. The effect of strain energy on growth rates during the 4 olivine-spinel transformation and implications for olivine metastability in subducting slabs. *Journal of Geophysical Ressearch* 103:23,897–23,909.

Mang C., Kontny A., Fritz J., and Schneider R. 2013. Shock experiments up to 30 GPa and their consequences on

microstructures and magnetic properties in pyrrhotite. *Geochemistry Geophysics Geosystems* 14:64–85.
McSween H. Y. 1999. *Meteorites and their parent planets*. 2nd ed. Cambridge: Cambridge University Press. 310 p.
Melosh H. J. 1984. Impact ejection, spallation, and the origin of meteorites. *Icarus* 59:234–260.
Melosh H. J. 1989. *Impact cratering: A geologic process*. New York: Oxford University Press. 253 p.
Meyer C., Fritz J., Misgaiski M., Stöffler D., Artemieva N. A., Hornemann U., Moeller R., de Vera J.-P., Cockell C., Horneck G., Ott S., and Rabbow R. 2011. Shock experiments in support of the Lithopanspermia theory: The influence of host rock composition, temperature and shock pressure on the survival rate of endolithic and epilithic microorganisms. *Meteoritics & Planetary Science* 46:701–718.
Ming L. C., Kim Y. H., Manghnani M. H., Usha-Devi S., Ito E., and Xie H. -S. 1991. Back transformation and oxidation of (Mg, $Fe)_2SiO_4$ spinels at high temperatures. *Physics and Chemistry of Minerals* 18:171–179.
Miyahara M., El Goresy A., Ohtani E., Nagase T., Nishijima M., Vashaei Z., Ferroir T., Gillet P., Dubrovinsky L., and Simionovici A. 2008. Evidence for fractional crystallization of wadsleyite and ringwoodite from olivine melts in chondrules entrained in shock-melt veins. *PNAS* 105:8542–8547.
Miyahara M., Ohtani E., Ozawa S., Kimura M., El Goresy A., Sakai T., Nagase T., Hiraga K., Hirao N., and Ohishi Y. 2011. Natural dissociation of olivine to (Mg, Fe)SiO3 perovskite and magnesiowüstite in a shocked Martian meteorite. *PNAS* 108:5999–6003.
Miyahara M., Kaneko S., Ohtani E., Sakai T., Nagase T., Kayama M., Nishido H., and Hirao N. 2013. Discovery of seifertite in a shocked lunar meteorite. *Nature Communications* 4:1737. doi:10.1038/ncomms2733.
Miyahara M., Ohtani E., El Goresy A., Ozawa S., and Gillet P. 2016. Phase transition processes of olivine in the shocked Martian meteorite Tissint: Clues to origin of ringwoodite-, bridgmanite- and magnesiowüstite-bearing assemblages. *Physics of the Earth and Planetary Interiors* 259:18–28.
Moser D. E., Chamberlain K. R., Tait K. T., Schmitt A. K., Darling J. R., Barker I. R., and Hyd B. C. 2013. Solving the Martian meteorite age conundrum using micro-baddeleyite and launch-generated zircon. *Nature* 499:454–457.
Müller W. F. and Hornemann U. 1969. Shock-induced planar deformation structures in experimentally shock-loaded olivines and in olivines from chondritic meteorites. *Earth and Planetary Science Letters* 7:251–264.
Ott U. 2007. Presolar grains in meteorites and their compositions. *Space Science Reviews* 130:87–95.
Quirico E., Montagnac G., Rouzaud J. N., Bonal L., Bourot-Denise M., Duber S., and Reynard B. 2009. Precursor and metamorphic condition effects on Raman spectra of poorly ordered carbonaceous matter in chondrites and coals. *Earth and Planetary Science Letters* 287:185–193.
Reynard B. and Rubie D. 1996. High-pressure, high-temperature Raman spectroscopic study of ilmenite-type $MgSi0_3$. *American Mineralogist* 81:1092–1096.
Reznik B., Kontny A., Fritz J., and Gerhards U. 2016. Shock-induced deformation phenomena in magnetite and their consequences on magnetic properties. *Geochemistry Geophysics Geosystems* 17:2374–2393. doi:10.1002/2016GC006338.
Rubin A. 2004. Postshock annealing and postannealing shock in equilibrated ordinary chondrites: Implications for the thermal and shock histories of chondritic asteroids. *Geochimica et Cosmochimica Acta* 68:673–689.
Rubin A. 2015. Maskelynite in asteroidal, lunar and planetary basaltic meteorites: An indicator of shock pressure during impact ejection from their parent bodies. *Icarus* 257:221–229.
Rubin A., Scott E. R. D., and Keil K. 1997. Shock metamorphism of enstatite chondrites. *Geochimica et Cosmochimica Acta* 61:847–858.
Schmitt R. T. 2000. Shock experiments with the H6 chondrite Kernouvè: Pressure calibration of microscopic shock effects. *Meteoritics & Planetary Science* 35:545–560.
Schmitz B., Tassinari M., and Peucker-Ehrenbrink B. 2001. A rain of ordinary chondritic meteorites in the early Ordovician. *Earth and Planetary Science Letters* 194:1–15.
Schwenzer S. P., Fritz J., Stöffler D., Trieloff M., Amini M., Greshake A., Herrmann S., Herwig K., Jochum K. P., Mohapatra R. K., Stoll B., and Ott U. 2008. Helium loss from Martian meteorites—Mainly induced by shock metamorphism: Evidence from new data and a literature compilation. *Meteoritics & Planetary Science* 43:1841–1859.
Scott E. R. D., Keil K., and Stöffler D. 1992. Shock metamorphism of carbonaceous chondrites. *Geochimica et Cosmochimica Acta* 56:4281–4293.
Sears D. W., Ashworth J. R., and Broadbent C. P. 1984. Studies of an artificially shock-loaded H group chondrite. *Geochimica et Cosmochimica Acta* 48:343–360.
Sharp T. G. and DeCarli P. S. 2006. Shock effects in meteorites. In *Meteorites and the early solar system II*, edited by Lauretta D. S. and McSween H. Y. Jr. Tucson, Arizona: University of Arizona Press. pp. 653–677.
Shuster D. L., Balco G., Cassata W. S., Fernandes V. A., Garrick-Bethell I., and Weiss B. P. 2010. A record of impacts preserved in the lunar regolith. *Earth and Planetary Science Letters* 290:155–165.
Snee L. W. and Ahrens T. J. 1975. Shock induced deformation features in terrestrial peridot and lunar dunite. Proceedings, 6th Lunar Planetary Science Conference. pp. 833–842.
Stöffler D. 1982. Density of minerals and rocks under shock compression. In *Landolt-Börnstein—Numerical data and functional relationships in science and technology*, edited by Angenheister G. Berlin: Springer. pp. 120–183.
Stöffler D. and Grieve R. A. F. 2007. Impactites. In *Metamorphic rocks: A classification and glossary of terms, recommendations of the International Union of Geological Sciences*, edited by Fettes D. and Desmons J. Cambridge, UK: Cambridge University Press. pp. 82–92, 111–125, and 126–242.
Stöffler D., Ostertag R., Jammes C., Pfannschmidt G., Sen Gupta P. R., Simon S. B., Papike J. J., and Beauchamp R. H. 1986. Shock metamorphism and petrography of the Shergotty achondrite. *Geochimica et Cosmochimica Acta* 50:889–903.
Stöffler D., Bischoff A., Buchwald V., and Rubin A. 1988. Shock effects in meteorites. In *Meteorites and the early solar system*, edited by. Kerridge J. F. and Matthews M. S. Tucson, Arizona: University of Arizona Press. pp. 165–202.
Stöffler D., Keil K., and Scott E. R. D. 1991. Shock metamorphism of ordinary chondrites. *Geochimica et Cosmochimica Acta* 55:3845–3867.

Swindle T. D., Isachsen C. E., Weirich J. R., and Kring D. A., 2009. ^{40}Ar–^{39}Ar ages of H chondrite impact melt breccias. *Meteoritics & Planetary Science* 44:747–762.

Taran M., Koch-Müller M., Wirth R., Abs-Wurmbach I., Rhede D., and Greshake A. 2009. Spectroscopic studies of synthetic and natural ringwoodite, γ-$(Mg, Fe)_2SiO_4$. *Physics and Chemistry of Minerals* 36:217–232.

Taylor G. J. and Heymann D. 1969. Shock, reheating, and the gas retention ages of chondrites. *Earth and Planetary Science Letters* 7:151–161.

Tomioka N. and Fujino K. 1997. Natural $(Mg, Fe)SiO_3$-ilmenite and -perovskite in the Tenham Meteorite. *Science* 277:1084–1086.

Trunin R. F., Gudarenko L. F., Zhernokletov M. V., and Simakov G. V. 2001. *Experimental data on shock compression and adiabatic expansion of condensed matter*. Sarov, Russia: Russian Federal Nuclear Center. 446 p.

Tschauner O., Ma C., Beckett J. R., Prescher C., Prakapenka V. B., and Rossman G. R. 2014. Discovery of bridgmanite, the most abundant mineral in Earth, in a shocked meteorite. *Science* 346:1100–1102.

Van de Moortèle B., Reynard B., Rochette P., Jackson M., Beck P., Gillet P., McMillan P. F., and McCammon C. A. 2007. Shock-induced metallic iron nanoparticles in olivine-rich Martian meteorites. *Earth and Planetary Science Letters* 262:37–49.

Van Schmus W. R. and Ribbe P. H. 1968. The composition and structural state of feldspar from chondritic meteorites. *Geochimica et Cosmochimica Acta* 32:1327–1342.

Wackerle J. 1962. Shock wave compression of quartz. *Journal of Applied Physics* 33:922–937.

Walton E. 2013. Shock metamorphism of Elephant Moraine A79001: Implications for olivine-ringwoodite transformation and the complex thermal history of heavily shocked Martian meteorites. *Geochimica et Cosmochimica Acta* 107:299–315.

Walton E., Sharp T., Hu J., and Filiberto J. 2014. Heterogeneous mineral assemblages in Martian meteorite Tissint as a result of a recent small impact event on Mars. *Geochimica et Cosmochimica Acta* 140:334–348.

Wasserburg G. J., Busso M., Gallino R., and Nollett K. M. 2006. Short-lived nuclei in the early solar system: Possible AGB sources. *Nuclear Physics A* 777:5–69.

Weiss B. P., Kirschvink J. L., Baudenbacher F. J., Vali H., Peters N. T., MacDonald F. A., and Wikswo J. P. 2000. A low temperature transfer of ALH84001 from Mars to Earth. *Science* 290:791–795.

Wittmann A., Swindle T. D., Cheek L. C., Frank E. A., and Kring D. A. 2010. Impact cratering on the H chondrite parent asteroid. *Journal of Geophysical Research: Planets* 115:E07009.

Wood J. 2005. The chondrite types and their origins. In *Chondrites and the protoplanetary disk*, edited by Krot A. N., Scott E. R. D., and Reipurth B. ASP conference series, 341. San Francisco, California: Astronomical Society of the Pacific. pp. 953–971.

Xie Z. and Sharp T. G. 2004. High-pressure phases in shock induced melt veins of the Umbarger L6 chondrite: Constraints on shock pressure. *Meteoritics & Planetary Science* 39:2043–2054.

Xie Z. and Sharp T. G. 2007. Host rock solid-state transformation in a shock-induced melt vein of Tenham L6 chondrite. *Earth and Planetary Science Letters* 254:433–445.

Xie X., Chen M., Dai C., El Goresy A., and Gillet P. 2001. A comparative study of naturally and experimentally shocked chondrites. *Earth and Planetary Science Letters* 187:345–356.

Xie Z., Sharp T. G., and DeCarli P. S. 2006a. High-pressure phases in a shock-induced melt vein of the Tenham L6 chondrite: Constraints on shock pressure and duration. *Geochimica et Cosmochimica Acta* 70:504–515.

Xie Z., Sharp T. G., and De Carli P. S. 2006b. Estimating shock pressures based on high-pressure minerals in shock-induced melt veins of L chondrites. *Meteoritics & Planetary Science* 41:1883–1898.